Research Article

ADVANCED PHOTONICS

Transmission of vector vortex beams in dispersive media

Ilaria Gianani,[a,b] Alessia Suprano,[a] Taira Giordani,[a] Nicolò Spagnolo,[a] Fabio Sciarrino,[a,c,*] Dimitris Gorpas,[d,e] Vasilis Ntziachristos,[d,e] Katja Pinker,[f] Netanel Biton,[g] Judy Kupferman,[g] and Shlomi Arnon[g]

[a]Sapienza Università di Roma, Dipartimento di Fisica, Rome, Italy
[b]Università degli Studi Roma Tre, Dipartimento di Scienze, Rome, Italy
[c]Consiglio Nazionale delle Ricerche, Istituto dei Sistemi Complessi, Roma, Italy
[d]Technische Universität München, Biological Imaging and Center for Translational Cancer Research, Munich, Germany
[e]Institute of Biological and Medical Imaging, Helmholtz Zentrum München, Neuherberg, Germany
[f]Medical University of Vienna, Department of Biomedical Imaging and Image-Guided Therapy, Molecular and Gender Imaging Service, Vienna, Austria
[g]Ben-Gurion University of the Negev, Department of Electrical and Computer Engineering, Beer Sheva, Israel

Abstract. Scattering phenomena affect light propagation through any kind of medium from free space to biological tissues. Finding appropriate strategies to increase the robustness to scattering is the common requirement in developing both communication protocols and imaging systems. Recently, structured light has attracted attention due to its seeming scattering resistance in terms of transmissivity and spatial behavior. Moreover, correlation between optical polarization and orbital angular momentum (OAM), which characterizes the so-called vector vortex beams (VVBs) states, seems to allow for the preservation of the polarization pattern. We extend the analysis by investigating both the spatial features and the polarization structure of vectorial optical vortexes propagating in scattering media with different concentrations. Among the observed features, we find a sudden swift decrease in contrast ratio for Gaussian, OAM, and VVB modes for concentrations of the adopted scattering media exceeding 0.09%. Our analysis provides a more general and complete study on the propagation of structured light in dispersive and scattering media.

Keywords: orbital angular momentum; scattering phenomena; turbulent media; optical polarization; vector vortex beams.

Received Feb. 14, 2020; revised manuscript received Apr. 29, 2020; accepted for publication May 7, 2020; published online May 22, 2020.

[DOI: 10.1117/1.AP.2.3.036003]

1 Introduction

The study of structured light is an important field of investigation in both the quantum and classical regimes.[1,2] In particular, light carrying orbital angular momentum (OAM) different from zero has been used in many applications ranging from quantum simulation[3,4] and quantum engineering[5,6] to quantum and classical communications.[7–14] Recently, OAM modes have been particularly studied for their uses in biomedical applications of imaging and diagnosis.[15–17] In particular, they have been exploited for the development of noninvasive diagnostics on tissues. In this regard, studies comparing the transmittance to the Gaussian spatial mode on scattering media simulating real tissue properties have been carried out.[18–20] In this context, it becomes of fundamental importance to investigate how the structure of OAM modes can be degraded by scattering and turbulent media. In particular, this has been investigated in communications through scattering media,[21] atmospheric turbulence,[22–24] and underwater.[25,26]

Increasing the complexity of the beam profile can lead to improved performances in turbulent media.[27–32] This can be achieved with vector vortex beams (VVBs), which are structured beam profiles in which the helicoidal wavefront is coupled with a nonuniform distribution of the polarization on the transverse plane. The coupling between these two degrees of freedom makes VVBs a suitable choice for several applications in the classical

*Address all correspondence to Fabio Sciarrino, E-mail: fabio.sciarrino@uniroma1.it

regime, such as microscopy,[33,34] optical tweezers,[35,36] energy-efficient metal-cutting lasers,[37] and classical communication.[38,39] Moreover, they find further application in the quantum regime for sensing and metrology,[40,41] quantum simulation,[3,4] and quantum communication.[7–9]

VVBs present a polarization pattern that also has to be addressed. Experiments investigating polarization preservation through scattering media of a VVB obtained by superposition of opposite OAM (± 1) modes have shown an enhancement by a factor of 2 compared with that of a Gaussian beam.[42] Furthermore, by analyzing the transmissivity behavior for circularly polarized Laguerre–Gauss (LG) modes and azimuthal or radial polarization patterns in VVB modes, a highest transmission for the radially polarized VVB was observed.[43] These considerations make VVBs a good candidate for improving the transmission in scattering media, towards the realization of *in vivo* diagnostic devices.

To employ VVB in realistic diagnostic devices, however, another fundamental aspect that requires investigation is the preservation of the mode spatial features after interaction with the scattering media. This has been studied with scalar fields carrying a topological charge and a uniform polarization profile, which have been shown, at moderate scattering lengths, to exhibit only a slight effect on the beam distortion.[44]

Here, we report on a similar analysis on VVB, further extending the scattering region. We study the spatial behavior of different VVBs and OAM modes going through scattering media composed of solutions of polystyrene latex beads with different concentrations. Our results provide indication of an abrupt spatial mode degeneration. Moreover, we extend the analysis presented in Ref. 42, by investigating the depolarization ratio (DR) of VVBs obtained from superposition of OAM modes with different values, comparing it with that of a Gaussian mode.

2 Experiment

Our experimental apparatus to investigate the scattering properties of dispersive media with structured light envisages three different stages. The first is designed for generating structured light as scalar optical vortexes carrying a defined amount of OAM and VVBs. Then, we have the samples and the detection stages to collect the scattered light and analyze its properties.

The OAM degree of freedom is associated with a helicoidal structured wavefront.[45,46] The state of a photon with nonzero OAM is described by LG modes. These modes are characterized by two parameters (m, p): the first is the azimuthal parameter associated with the OAM value and the latter is the radial parameter associated with the radial intensity distribution. To generate OAM modes, we adopt the system used in Ref. 6, described in Fig. 1, which makes use of five q-plates[47,48] combined with half-waveplates (HWPs) to obtain OAM modes going from -5 to 5. Indeed q-plates are inhomogeneous birefringent media in which the orientation of the optical axis is not uniform in the slab's plane. The resulting pattern is periodical around a singularity in the origin of the plane, with a winding number expressed by the topological charge q. Consequently, such plates impress different phase retardation to the wavefront according to the coordinates in the transverse plane and conditionally to the polarization states, generating optical vortexes with charges equal to $2q$. More precisely, the action of a single q-plate on a circular polarized vortex, with a topological charge equal to m, can be summarized as follows:

$$\begin{bmatrix} |m,L\rangle \\ |m,R\rangle \end{bmatrix} \overset{q-\text{plate}}{\rightarrow} \begin{bmatrix} |m+2q,R\rangle \\ |m-2q,L\rangle \end{bmatrix}, \tag{1}$$

or, in terms of the q-plate transfer matrix in the R, L basis

$$\begin{bmatrix} |m,L\rangle \\ |m,R\rangle \end{bmatrix} \overset{q-\text{plate}}{\rightarrow} \begin{bmatrix} 0 & e^{-2iq\phi} \\ e^{2iq\phi} & 0 \end{bmatrix} \begin{bmatrix} |m,L\rangle \\ |m,R\rangle \end{bmatrix}. \tag{2}$$

The device generates vectorial fields when, for instance, the incident beam is linearly polarized. In this case, the output field is a VVB that is the superposition of two optical vortexes with opposite charges and orthogonal polarization.[48] This scheme can be generalized using cascaded q-plates and waveplates for generating VVBs in the form

$$|\Psi_{m_1,m_2,p}\rangle = \cos\frac{\theta}{2}|m_1,L\rangle + e^{i\phi}\sin\frac{\theta}{2}|m_2,R\rangle, \tag{3}$$

where $\theta \in [0,\pi]$, $\phi \in [0,2\pi]$, and m_1 and m_2 will take all of the odd values in the interval $[-5,5]$. It is worth noting that the states in Eq. (3) could generate different types of structured light. These include vectorial fields as well as coherent superpositions of optical vortexes with m_1 and m_2 after suitable polarization projections and single vortexes when these projections are set to a circular basis. Indeed, the adopted cascaded q-plates scheme allows for the generation of VVBs resulting from the superposition of modes carrying different topological charges. Furthermore, such an apparatus avoids the need for interferometric setups to generate such a class of OAM-polarization superposition states.[49] The flexibility of this apparatus allows for the investigation of the response of our sample under the illumination of different structured beams. In our implementation, we aim at generating balanced VVBs ($\theta = \frac{\pi}{2}$). However, some discrepancies will arise due to misalignment in the setup; ϕ will be equal to 0 or π depending on the generated mode.

To generate such states, we employ a continuous wave (CW) laser (CNI laser PSU-III-FDA) at 808 nm opportunely shaped by the apparatus shown in Fig. 1, which is then sent through the sample. The scattering medium is a solution of polystyrene latex beads (Sigma-Aldrich) with diameter $d = 3.12\ \mu\text{m}$ in distilled water with varying concentrations from 0.05% to 0.12%. The choice of such a scattering medium is motivated by the possibility of accessing different scattering regimes via its concentration. Furthermore, our analysis is intended to thoroughly extend previous studies performed with the same scattering system.[18,19,42] The sample is placed in a Hellma quartz cuvette with a fixed path length $L = 1$ cm. The concentrations are reported in Table 1 together with the scattering length, as well as the scattering and the attenuation coefficients.

The last part of our apparatus consists of the collection and analysis of the scattered light. A CCD camera (Thorlabs BC106N-VIS/M) records the images in the far field after a $20\times$ objective. A polarization analysis stage, made by a quarter-waveplate (QWP) and HWP followed by a polarizing beam-splitter (PBS) cube, is eventually placed before the objective.

In this work, we address both the spatial and polarization properties of the vector beams after propagation in the scattering medium. To perform the spatial analysis, we select the central slice of the mode, averaged over 50 acquisitions, and we compute the contrast ratio given as

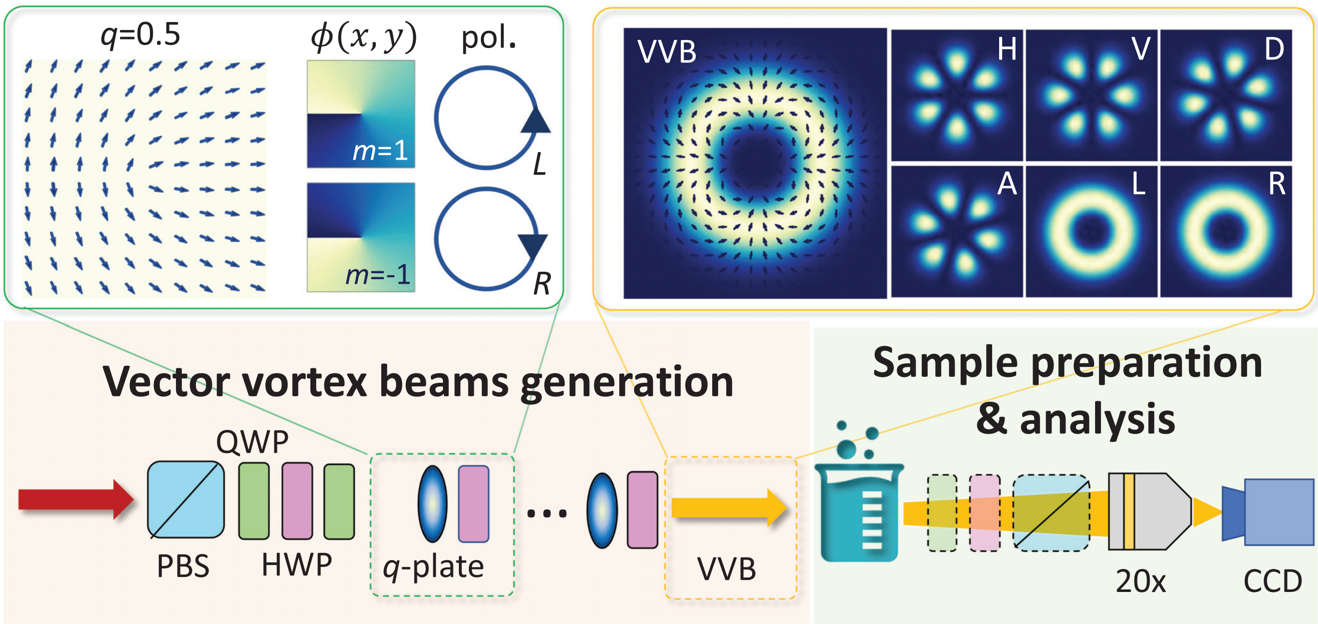

Fig. 1 Experimental scheme. A CW laser emits a Gaussian beam with $m = 0$, at 808 nm. Then, the preparation stage for the initial polarization state is made with a PBS, QWP, and HWP. Five units, each composed of a q-plate (oval blue symbol) followed by an HWP (pink rectangle), generate structured light. Our q-plates display a charge $q = 0.5$, which increases (decreases) the OAM number by 1. In the inset, we report the optical axis orientation of the plate and the phase acquired by the wavefront in the transverse plane $\phi(x, y)$ conditionally to the polarization states (L, R). After this preparation stage, we obtain VVBs in the form of Eq. (2), shown in the second inset of the figure (H, horizontal polarization; V, vertical polarization; D, diagonal polarization; A, antidiagonal polarization; L, left circular polarization; and R, right circular polarization). Depending on the analysis, we can use the whole vectorial field or the scalar fields produced by a suitable projection of the polarization on the basis b. The second stage consists of the sample, prepared with several concentrations of latex beads, and the detection platform. An objective collects the scattered light and focuses the image on the CCD camera. A polarization analyzer can be inserted between the sample and the objective.

$$C = \frac{\bar{I}_{\max} - I_{\min}}{\bar{I}_{\max}}, \tag{4}$$

where $\bar{I}_{\max}$ is the average between peaks of the two lobes of the ring-mode and $I_{\min}$ is the central minimum value. These values are obtained by performing a fit with a double Gaussian function on the averaged central slice of the mode. The analysis on the Gaussian modes, both linearly and circularly polarized, is performed in a similar fashion, but $\bar{I}_{\max}$ corresponds to the peak of the mode and $I_{\min}$ is the background noise, and these are obtained by performing a Gaussian fit.

Table 1 Scattering properties of latex beads. The relevant parameters of our scattering samples are reported, namely the scattering length l_s, transmission length l_{tr}, scattering coefficient μ_s, the inverse of transmission length μ_s', the scattering anisotropic coefficient g, and the quantity $\mu_s L$, where $L = 1$ cm is the sample length. Those parameters are determined to provide a complete picture of the scattering conditions corresponding to the performed experimental tests. The values were retrieved for different concentrations $\mathcal{C}$ of latex beads. The calculations were obtained using the program available in Ref. 50.

$\mathcal{C}$ (%)	l_s (μm)	l_{tr} (μm)	$\mu_s = 1/l_s$ (cm^{-1})	$\mu_s' = 1/l_{tr}$ (cm^{-1})	g	$\mu_s L$
0.05	1507	14,527	6.63	0.69	0.896	6.63
0.08	942	9079	10.61	1.10	0.896	10.61
0.09	838	8070	11.19	1.24	0.896	11.19
0.10	754	7263	13.2	1.38	0.896	13.2
0.11	686	6603	14.6	1.51	0.896	14.6
0.12	629	6053	15.9	1.65	0.896	15.9

We adopt the contrast ratio as a criterion for identifying the spatial resolution limit as it provides a clear indication on whether the spatial features of the mode can be distinguished by the detection device.

Conversely, the polarization analysis is performed by estimating the DR for the VVBs and for the Gaussian mode. To this aim, measurements on a polarization basis $b = \{(H,V),(D,A),(L,R)\}$ resolved in the coordinates (x,y) of the transverse plane allow for the retrieval of the set of Stokes parameters:

$$S_1 = \frac{I_H - I_V}{I_H + I_V}; \quad S_2 = \frac{I_D - I_A}{I_D + I_A}; \quad S_3 = \frac{I_R - I_L}{I_R + I_L}, \tag{5}$$

where I_b represents the intensity associated with the element of the basis b. The DR is then defined as

$$\mathrm{DR} = \sqrt{(S_1)^2 + (S_2)^2 + (S_3)^2}. \tag{6}$$

This means that every fully polarized light will have $\mathrm{DR} = 1$ regardless of the polarization direction, whereas the DR will decrease to 0 for unpolarized light.

3 Results

In the following, we report the results of our analysis regarding the scattering effects on the spatial and polarization properties of VVBs.

The first study reports the behavior of the contrast C introduced in the previous section, for different concentrations of latex beads in the water solution. This analysis was carried out to investigate the spatial resolution after diffusion in the

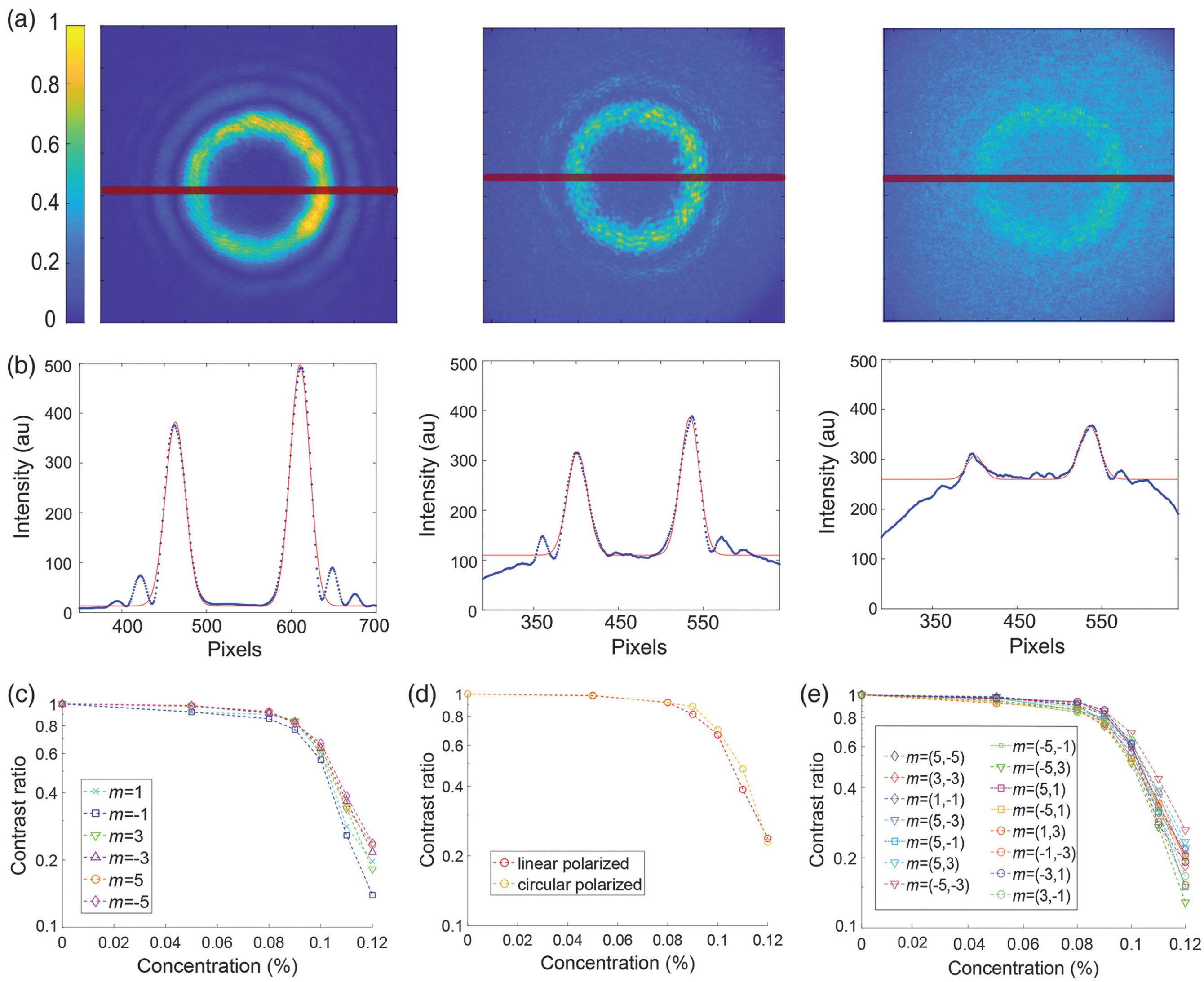

Fig. 2 Contrast analysis. (a) Recorded beam profiles associated with OAM 5 for three different concentrations $\mathcal{C} = 0\%$, 0.10%, 0.12%. In each image, the red line indicates the selected slice for the fitting procedure. (b) Fit on the selected slices, for the same concentration of the above panel. Contrast ratio in a logarithmic scale for (c) circularly polarized OAM modes, (d) linearly and circularly polarized Gaussian modes, and (e) several VVBs modes as a function of the beads concentration, respectively.

medium. Instead of two separate light sources, we directly address two different, separate parts of the same mode. To do so, we use the two intensity peaks along the x axis in the image plane to retrieve C as a quantifier of the resolution power. In Fig. 2, we report some pictures of the peaks profile after the sample along with the trend of C for the OAM mode with $m = 5$ at $\mathcal{C} = 0\%$, 0.10%, 0.12%. Similar analysis was carried out for all circularly polarized OAMs and VVBs considered and for both linearly and circularly polarized Gaussian modes. In the peaks profile analysis, we observe two contributions in the images. The first one resembles the vortex structure in which we observe an attenuation of the signal. However, this is not associated with a broadening of the spatial components. Indeed this contribution is due to the photons that have not been scattered multiple times by the material. As such, for this component we do not observe a significant deterioration of the spatial correlation of the original VVB. We observe that there is a slight asymmetry in the peaks' intensity, which is due to the alignment of the cascaded q-plates. The second contribution is the background given by the scattered photons that have lost the spatial information. The same investigation was performed for increasing values of concentration $\mathcal{C}$ of scattered centers in the liquid solution. We observe that, since there is no broadening of the spatial features, the only effect here is that of a reduced intensity of the transmitted beam: all modes seem to be affected equally by this behavior.

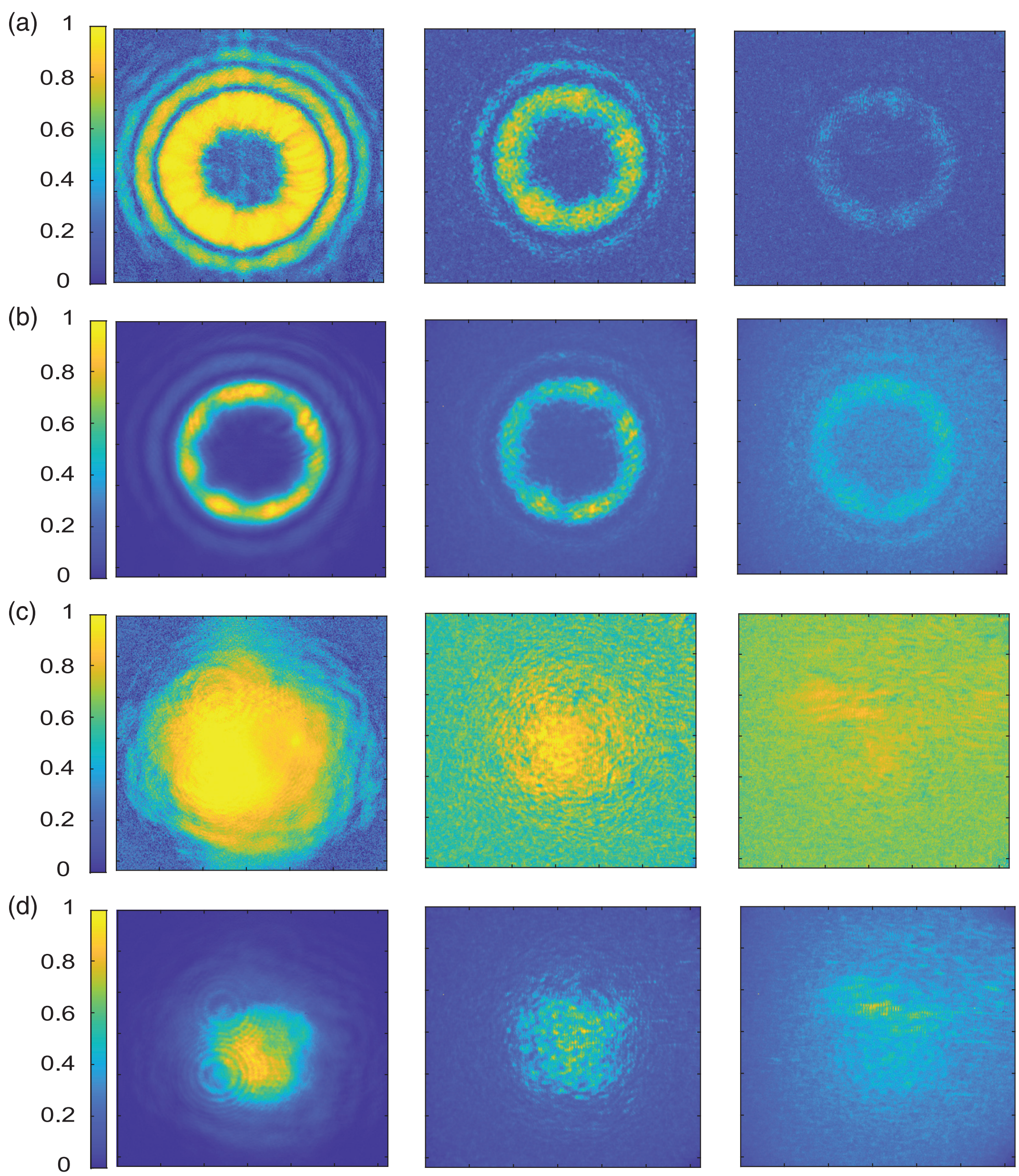

Fig. 3 Depolarization analysis. (a) Pixel-by-pixel DR for the VVB mode with $m_1 = 5$ and $m_2 = -5$, for three different concentrations $\mathcal{C} = 0\%$, 0.10%, 0.12%. (b) Spatial profile of the same mode for comparison. (c) Pixel-by-pixel DR for a circularly polarized Gaussian mode, for three different concentrations $\mathcal{C} = 0\%$, 0.10%, 0.12%. (d) Spatial profile of the same mode for comparison.

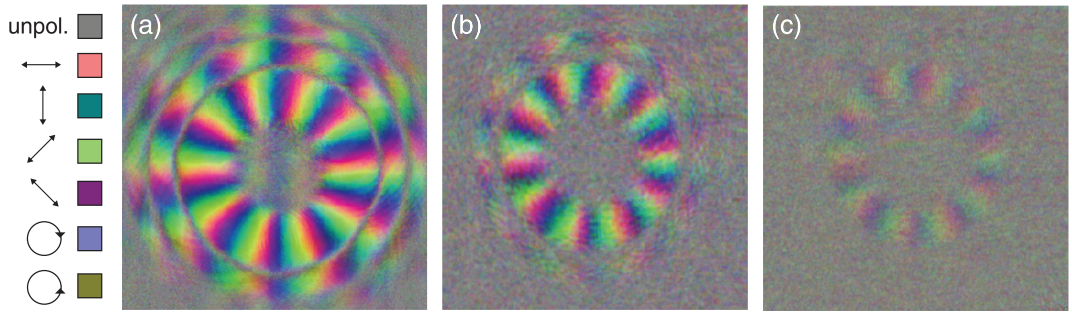

Fig. 4 Polarization pattern analysis. RGB map of the Stokes parameters for the VVB mode with $m_1 = 5$ and $m_2 = -5$, for three different concentrations $\mathcal{C} = 0\%$, 0.10%, 0.12%.

We performed the analysis for different concentrations, ranging from very small values to the point where we could not detect any residual transmitted mode on the camera. This happened for concentrations higher than 0.12%. In Figs. 2(c)–2(e), we report the behaviors for all analyzed modes. We observe that the contrast has a plateau up to $\mathcal{C} \simeq 0.09\%$ and then it abruptly decreases.

The second investigated aspect concerns preservation of the light polarization features. This point is crucial in the presence of VVBs, which have a particular property of displaying well-defined polarization patterns. To measure the DR, we illuminated the sample with different VVBs states and performed the polarization measurements discussed in the previous section. Figure 3 shows the pixel-by-pixel DR for the circularly polarized Gaussian mode and for the VVB given by the superposition of $m_1 = 5$ and $m_2 = -5$ as an example. From this, we observe that the component related to the scattering is strongly depolarized for the VVBs, whereas it maintains the original circular polarization for the Gaussian mode. The unperturbed component instead maintains a high degree of polarization in both instances (the slight decrease in the VVB is to be attributed to the scattering background overlapped to the unperturbed signal). The same results were obtained for all of the VVBs considered and for the linearly polarized Gaussian mode, respectively. A possible interpretation of this result is that, while the Gaussian polarization pattern is flat, the VVBs one is highly structured. Hence, as the light is scattered, in the same propagation direction k, it might occur that different polarizations are incoherently superimposed, resulting in a low value of DR. This cannot happen with the Gaussian profile since there is no spatial dependence on the polarization to begin with.

To study the behavior of the polarization pattern, we also address individually the Stokes parameters. We associate an RGB map with the three Stokes parameters to visualize the polarization pattern in a single image. This is shown in Fig. 4 for the same concentrations $\mathcal{C}$ chosen for the DR of the VVB given by the superposition of $m_1 = 5$ and $m_2 = -5$, as before. The pattern is clearly defined for the nonscattered mode, and it is retained up to the highest concentration for the portion of beam that is also spatially unaffected by the scattering. Conversely, all of the scattered light is completely mixed, and the polarization correlations are lost.

4 Discussion

In this paper, we investigated the propagation of structured light through dispersive media. More specifically, we performed a thorough analysis on how the optical properties of complex spatial profiles are affected by the scattering process in a turbulent environment. This was realized by means of micrometric latex beads in a water solution at different concentrations. We focused our analysis on two specific tasks, namely the study of spatial contrast degradation and depolarization of the input beam. To this end, with a flexible apparatus, we generated different input modes, ranging from OAM valued beams to VVBs carrying correlation between polarization and spatial profile.

Concerning the investigation on the contrast degradation in the spatial profile, we observe that OAM carrying beams are characterized by an abrupt change in the resolution. In particular, spatial profiles are maintained up to a certain threshold concentration of $\mathcal{C} \sim 0.09\%$, analogously to that observed in former papers.[44] Conversely, a fast contrast degradation is observed for higher concentrations. Furthermore, the behavior and the threshold are shown to be almost independent of the OAM values in the investigated regime. However, we observe from Fig. 2 that a slight difference in contrast ratio for OAM values is present. Additional studies are needed to clarify this phenomenon. Therefore, investigation of this aspect could be done both for higher concentrations and for a far greater range of OAM values. The same results are obtained for VVBs and for Gaussian inputs. Moreover, we observe that the spatial profile of the unscattered light preserves the original intensity distribution.

The second analysis focused on verifying the polarization degradation of the input beams. This investigation is particularly relevant for VVB states due to their correlated and complex spatial-polarization profiles. A study of the same effect has been performed in Ref. 42, for two order of magnitude shorter sample thicknesses and with a single VVB with $m = \pm 1$. For the concentrations and the investigated sample length, we observe two different behaviors for Gaussian inputs and VVBs. More specifically, the former states present a uniform polarization profile that is unaffected by the scattering process. An entirely different behavior is observed for VVBs. Indeed, for this class of states, we find that the light portion that has undergone multiple scattering is completely unpolarized, while the coherent part that has not interacted with the medium maintains its polarization pattern. These results provide the first comprehensive analysis covering different concentrations and mode profiles, in both the spatial and polarization degrees of freedom, and can help in establishing a framework for application of structured light illumination in imaging and communications protocols. Furthermore, these results stimulate further research on the behavior of structured light undergoing scattering processes, including investigating the effect on different media mimicking tissue-like features.

Acknowledgments

This project received funding from the European Union's Horizon 2020 research and innovation program (Future and Emerging Technologies) under Grant Agreement No. 828978.

References

1. L. Marrucci et al., "Spin-to-orbital conversion of the angular momentum of light and its classical and quantum applications," *J. Opt.* **13**, 064001 (2011).
2. M. Erhard et al., "Twisted photons: new quantum perspectives in high dimensions," *Light Sci. Appl.* **7**, 17146 (2018).
3. F. Cardano et al., "Statistical moments of quantum-walk dynamics reveal topological quantum transitions," *Nat. Commun.* **7**, 11439 (2016).
4. F. Cardano et al., "Detection of ZAK phases and topological invariants in a chiral quantum walk of twisted photons," *Nat. Commun.* **8**, 15516 (2017).
5. L. Innocenti et al., "Quantum state engineering using one-dimensional discrete-time quantum walks," *Phys. Rev. A* **96**, 062326 (2017).
6. T. Giordani et al., "Experimental engineering of arbitrary qudit states with discrete-time quantum walks," *Phys. Rev. Lett.* **122**, 020503 (2019).
7. D. Cozzolino et al., "Air-core fiber distribution of hybrid vector vortex-polarization entangled states," *Adv. Photonics* **1**(4), 046005 (2019).
8. A. Sit et al., "High-dimensional intracity quantum cryptography with structured photons," *Optica* **4**, 1006–1010 (2017).
9. G. Vallone et al., "Free-space quantum key distribution by rotation-invariant twisted photons," *Phys. Rev. Lett.* **113**, 060503 (2014).
10. D. Cozzolino et al., "Orbital angular momentum states enabling fiber-based high-dimensional quantum communication," *Phys. Rev. Appl.* **11**, 064058 (2019).
11. J. Kupferman and S. Arnon, "Decision algorithm for data center vortex beam receiver," *J. Opt.* **19**, 125702 (2017).
12. J. Kupferman and S. Arnon, "Direct detection receiver for vortex beam," *J. Opt. Soc. Am. A* **35**, 1543–1548 (2018).
13. J. Kupferman and S. Arnon, "Decoding algorithm for vortex communications receiver," *J. Opt.* **20**, 015702 (2017).
14. J. Kupferman and S. Arnon, "OWC with vortex beams in data center networks," *Proc. SPIE* **10437**, 1043705 (2017).
15. L. Shi, A. Rodríguez-Contreras, and R. R. Alfano, "Gaussian beam in two-photon fluorescence imaging of rat brain microvessel," *J. Biomed. Opt.* **19**(12), 126006 (2014).
16. L. Shi et al., "Propagation of Gaussian and Laguerre–Gaussian vortex beams through mouse brain tissue," *J. Biophotonics* **10**(12), 1756–1760 (2017).
17. Y. Zhou et al., "Efficient two-photon excitation by photonic dimers," *Opt. Lett.* **44**, 475–478 (2019).
18. B. Cochenour et al., "Propagation of modulated optical beams carrying orbital angular momentum in turbid water," *Appl. Opt.* **55**, C34–C38 (2016).
19. W. B. Wang et al., "Deep transmission of Laguerre–Gaussian vortex beams through turbid scattering media," *Opt. Lett.* **41**, 2069–2072 (2016).
20. Z. Chen, Y. Zhou, and J.-T. Shen, "Photon antibunching and bunching in a ring-resonator waveguide quantum electrodynamics system," *Opt. Lett.* **41**, 3313–3316 (2016).
21. L. Gong et al., "Optical orbital-angular-momentum-multiplexed data transmission under high scattering," *Light Sci. Appl.* **8**, 27 (2019).
22. C. Gopaul and R. Andrews, "The effect of atmospheric turbulence on entangled orbital angular momentum states," *New J. Phys.* **9**(4), 94 (2007).
23. M. Krenn et al., "Communication with spatially modulated light through turbulent air across Vienna," *New J. Phys.* **16**(11), 113028 (2014).
24. M. Krenn et al., "Twisted light transmission over 143 km," *Proc. Natl. Acad. Sci. U. S. A.* **113**(48), 13648–13653 (2016).
25. F. Bouchard et al., "Quantum cryptography with twisted photons through an outdoor underwater channel," *Opt. Express* **26**(17), 22563–22573 (2018).
26. F. Hufnagel et al., "Characterization of an underwater channel for quantum communications in the Ottawa river," *Opt. Express* **27**(19), 26346–26354 (2019).
27. H. Rubinsztein-Dunlop et al., "Roadmap on structured light," *J. Opt.* **19**, 013001 (2017).
28. Y. Yuan et al., "The orbital angular momentum spreading for cylindrical vector beams in turbulent atmosphere," *IEEE Photonics J.* **9**(2), 6100610 (2017).
29. W. Cheng, J. W. Haus, and Q. Zhan, "Propagation of vector vortex beams through a turbulent atmosphere," *Opt. Express* **17**, 17829–17836 (2009).
30. M. Cheng et al., "Enhanced vortex beams resistance to turbulence with polarization modulation," *J. Quant. Spectrosc. Radiat. Transfer* **227**, 219–225 (2019).
31. Z. Chen, Y. Zhou, and J.-T. Shen, "Exact dissipation model for arbitrary photonic Fock state transport in waveguide QED systems," *Opt. Lett.* **42**, 887–890 (2017).
32. Z. Chen, Y. Zhou, and J.-T. Shen, "Entanglement-preserving approach for reservoir-induced photonic dissipation in waveguide QED systems," *Phys. Rev. A* **98**, 053830 (2018).
33. B. Sick, B. Hecht, and L. Novotny, "Orientational imaging of single molecules by annular illumination," *Phys. Rev. Lett.* **85**, 4482–4485 (2000).
34. F. Lu, W. Zheng, and Z. Huang, "Coherent anti-Stokes Raman scattering microscopy using tightly focused radially polarized light," *Opt. Lett.* **34**, 1870–1872 (2009).
35. J. Li, M. Zhang, and D. Wang, "Adaptive demodulator using machine learning for orbital angular momentum shift keying," *IEEE Photonics Technol. Lett.* **29**(17), 1455–1458 (2017).
36. J. Ng, Z. Lin, and C. T. Chan, "Theory of optical trapping by an optical vortex beam," *Phys. Rev. Lett.* **104**, 103601 (2010).
37. A. V. Nesterov and V. G. Niziev, "Laser beams with axially symmetric polarization," *J. Phys. D Appl. Phys.* **33**, 1817–1822 (2000).
38. G. Milione et al., "4×20 gbit/s mode division multiplexing over free space using vector modes and a q-plate mode (de)multiplexer," *Opt. Lett.* **40**, 1980–1983 (2015).
39. N. Bozinovic et al., "Terabit-scale orbital angular momentum mode division multiplexing in fibers," *Science* **340**(6140), 1545–1548 (2013).
40. V. D'Ambrosio et al., "Complete experimental toolbox for alignment-free quantum communication," *Nat. Commun.* **3**, 961 (2012).
41. R. Fickler et al., "Quantum entanglement of high angular momenta," *Science* **338**(6107), 640–643 (2012).
42. A. Doronin et al., "Propagation of cylindrical vector laser beams in turbid tissue-like scattering media," *Photonics* **6**(2), 56 (2019).
43. S. Mamani et al., "Transmission of classically entangled beams through mouse brain tissue," *J. Biophotonics* **11**(12), e201800096 (2018).
44. K. S. Morgan et al., "Free space propagation of concentric vortices through underwater turbid environments," *J. Opt.* **18**, 104004 (2016).
45. L. Allen et al., "Orbital angular momentum of light and the transformation of Laguerre–Gaussian laser modes," *Phys. Rev. A* **45**, 8185–8189 (1992).
46. M. Padgett, J. Courtial, and L. Allen, "Light's orbital angular momentum," *Phys. Today* **57**(5), 35 (2004).
47. L. Marrucci, C. Manzo, and D. Paparo, "Optical spin-to-orbital angular momentum conversion in inhomogeneous anisotropic media," *Phys. Rev. Lett.* **96**, 163905 (2006).
48. F. Cardano et al., "Polarization pattern of vector vortex beams generated by q-plates with different topological charges," *Appl. Opt.* **51**, C1–C6 (2012).

49. B. Ndagano et al., "Creation and detection of vector vortex modes for classical and quantum communication," *J. Lightwave Technol.* **36**(2), 292–301 (2018).
50. L. Instruments, "Scattering length calculator for Mie spheres," http://intranet.lsinstruments.ch:8080/lstar/lstar.php.

Ilaria Gianani received her Doctor of Philosophy degree from the University of Oxford, and is a postdoctoral fellow at the Sapienza Università di Roma and a visiting postdoctoral fellow at Università degli Studi Roma Tre. Her current main interests are quantum metrology and time-frequency correlations in SPDC sources.

Alessia Suprano is a PhD student in the Quantum Information Laboratory of Professor Fabio Sciarrino. Her current interests are focused on quantum optics for the implementation and exploitation of quantum walks in the orbital angular momentum degree of freedom of photons. She graduated in October 2018 at the Sapienza Università di Roma.

Taira Giordani received her PhD in 2020 from the Physics Department of Sapienza University of Rome. Her works have been focused in the development of machine learning and optimization methods for the certification and engineering of photonic quantum walks platforms.

Nicolò Spagnolo received his PhD in 2012 in physical science of matter, with a thesis on experimental multiphoton quantum optical states. He is a temporary researcher in the Department of Physics of Sapienza Università di Roma. His research interests are experimental quantum information, quantum simulation and quantum metrology protocols, implemented by adopting different photonic platforms.

Fabio Sciarrino received his PhD in 2004 with a thesis in experimental quantum optics. He is a full professor and head of the Quantum Information Lab in the Department of Physics of Sapienza Università di Roma. Since 2013, he has been a fellow of the Sapienza School for Advanced Studies. His main field of research is quantum information and quantum optics, with works on quantum teleportation, optimal quantum machines, fundamental tests, quantum communication, and orbital angular momentum.

Dimitris Gorpas obtained a PhD in engineering from the Technical University of Athens, Greece. Since 2016, he is leading the Fluorescence Imaging Group at the Chair of Biological Imaging and Center for Translational Cancer Research (TranslaTUM) of the Technical University of Munich, as well as the affiliated Institute for Biological and Medical Imaging at the Helmholtz Zentrum München. His scientific interests include the development of medical imaging systems, their clinical validation, and surgical guidance through optical measurements.

Vasilis Ntziachristos obtained his PhD from the University of Pennsylvania. He then served as instructor, assistant professor, and director of the Laboratory for Bio-Optics and Molecular Imaging at Harvard University and Massachusetts General Hospital. In 2007, he was appointed director of the Chair of Biological Imaging at TUM and director of the Institute of Biological and Medical Imaging at the Helmholtz Zentrum München. He is the director of bioengineering of the Helmholtz Pioneer Campus.

Katja Pinker is professor of radiology, attending at the Department of Biomedical Imaging and Image-Guided Therapy at the Medical University of Vienna and the Department of Radiology/Breast Services at the Memorial Sloan-Kettering Cancer Center. She is an expert in translational and clinical breast and oncologic gender imaging. Her research focuses on the clinical and experimental investigation of functional imaging to diagnose cancer, earlier, more accurate, minimal and/or noninvasively.

Netanel Biton is a graduate student in the Department of Electrical and Computer Engineering at Ben Gurion University (BGU), Israel, in the group of Professor Shlomi Arnon. His research involves a combination of optics and deep learning.

Judy Kupferman is a researcher at the Department of Electrical and Computer Engineering at Ben Gurion University (BGU), Israel, in the group of Professor Shlomi Arnon. She has published papers on quantum communication, physics and optical engineering. She is also a recognized expert in lighting design, which she taught for many years at Tel Aviv University.

Shlomi Arnon is a professor at the Department of Electrical and Computer Engineering at Ben Gurion University (BGU), Israel. His honors and awards include SPIE fellow and Fulbright fellow. His research has produced more than eighty journal papers in the area of optical engineering and associated fields. He is coordinator of the FET-OPEN cancer scan project.